

# Three-Way Serpentine Slow-Wave Structures with Stationary Inflection Point and Enhanced Interaction Impedance

Robert Marosi, *Student Member, IEEE*, Tarek Mealy *Student Member, IEEE*, Alexander Figotin,  
and Filippo Capolino, *Fellow, IEEE*

**Abstract**—We introduce two novel variants of the serpentine waveguide slow-wave structure (SWS), often utilized in millimeter-wave traveling-wave tubes (TWTs), with an enhanced interaction impedance. Using dispersion engineering in conjunction with transfer matrix methods, we tune the guided wavenumber dispersion relation to exhibit stationary inflection points (SIPs), and also non-stationary, or “tilted” inflection points (TIPs), within the dominant  $TE_{10}$  mode of a rectangular waveguide. The degeneracy is found below the first upper band-edge associated with the bandgap where neighboring spatial harmonics meet in the dispersion of the serpentine waveguide (SWG) which is threaded by a beam tunnel.

The structure geometries are optimized to be able to achieve an SIP which allows for three-mode synchronism with an electron beam over a specified wavenumber interval in the desired Brillouin zone. Full-wave simulations are used to obtain and verify the existence of the SIP in the three-way coupled waveguide and fine-tune the geometry such that a beam would be in synchronism at or near the SIP. The three-way waveguide SWS exhibits a moderately high Pierce impedance in the vicinity of a nearly-stationary inflection point, making the SWS geometry potentially useful for improving the power gain and basic extraction efficiency of millimeter-wave TWTs. Additionally, the introduced SWS geometries have directional coupler-like behavior, which enables distributed power extraction at frequencies near the SIP frequency.

**Index Terms**—serpentine waveguide (SWG), serpentine ladder waveguide (SLWG), three-coupled serpentine waveguide (TC-SWG), traveling-wave tube (TWT), millimeter-wave, dispersion, stationary inflection point (SIP), distributed power extraction (DPE), interaction impedance.

## I. INTRODUCTION

TRAVELING-WAVE tubes (TWTs) are able to perform broadband, high-power amplification due to the distributed transfer of energy from a beam of electrons to guided electromagnetic fields. There are two primary factors that control the strength of the interaction between the beam and the electromagnetic field: velocity synchronization between the beamline and guided modes and beam-wave interaction impedance, also called Pierce impedance, in the TWT slow wave structure (SWS) [1]. In S-band helix TWTs, Pierce

impedance is typically on the order of  $100 \Omega$ , allowing for efficient basic beam-wave power conversion. However, at millimeter-wave frequencies, microfabricated slow-wave structures such as the serpentine waveguide (SWG) typically exhibit Pierce (or interaction) impedance on the order of  $10 \Omega$  or smaller, which drastically reduces their basic conversion efficiency. This is partly due to the fact that serpentine-type TWTs are typically synchronized to an electron beam in the first or second Brillouin zone rather than the fundamental Brillouin zone to avoid the use of relativistic electron beam velocities which require much larger voltages to accelerate electrons close to the speed of light [2]. Due to structure geometry that scales inversely with operating frequency, helix-type TWTs become extremely difficult to fabricate at millimeter-wave frequencies, making microfabricated structures like the SWG much more attractive. In this paper, we propose two new types of dispersion-engineered SWSs based on the SWG geometry that are capable of exhibiting moderately high Pierce impedance over narrow bandwidths and can be microfabricated. These two structure variants, the serpentine ladder waveguide (SLWG) and the three-coupled serpentine waveguide (TCSWG), with their longitudinal cross-sections illustrated in Figs. 1a and 1b, respectively, can have their geometries easily designed to exhibit stationary inflection points (SIPs) or nearly-stationary tilted inflection points (TIPs), sometimes referred to as tilted SIPs, at specific frequencies, similarly to the kind shown in Fig. 1c. Such structures with SIPs are capable of exhibiting moderately high to very high Pierce (interaction) impedance comparable to the impedance observed near the band-edge of SWG SWS, where the group velocity and power flow also vanish. Therefore, at the frequencies that the electron beam is in synchronism with the SIP, we expect the proposed SIP SWS to also have a high Pierce gain parameter, as  $C^3 = Z_{\text{Pierce}} I_0 / (4V_0)$ , where  $I_0$  and  $V_0$  are the average current and equivalent kinetic voltage of the electron beam, respectively. These structures have potential use in the design of compact, high efficiency, millimeter-wave TWTs and backward-wave oscillators (BWOs).

The SIP is a class of modal degeneracy, whereby three eigenmodes coalesce in both their wavenumbers and eigenvectors (polarization states). Such modal degeneracies of orders 2, 3, and 4 were originally investigated by Figotin and Vitebskiy in [3]–[8]. The SIP is a particular type of exceptional point of degeneracy (EPD), and is sometimes called a “frozen mode” in

Robert Marosi, Tarek Mealy, and Filippo Capolino are with the Department of Electrical Engineering and Computer Science, University of California, Irvine, Irvine, California, e-mail: rmarosi@uci.edu tmealy@uci.edu f.capolino@uci.edu.

Alexander Figotin is with the Department of Mathematics, University of California, Irvine, Irvine, California, e-mail: afigotin@uci.edu.

literature. Exceptional points of degeneracy of various orders have been previously investigated theoretically in gainless and lossless structures operating at both radio and optical frequencies in [9]–[22], and have also been experimentally demonstrated at radio frequency in [23]–[28]. In particular, the first experimental demonstration of SIPs at radio frequencies in a reciprocal three-way waveguide SWS has been performed in [28]. The slow wave structures we introduce here are designed to operate with an electron beam synchronized to three degenerate “cold” eigenmodes. That is, the SIP is made to exist in the “cold” dispersion relation, i.e., before the introduction of an electron beam, which will perturb the dispersion relation. Note that this regime of operation is different from the regime of “exceptional synchronization” or “degenerate synchronization” studied in [29]–[31], where an exceptional point of degeneracy is designed to occur in the “hot” system, i.e., it is visible only in the hot modal dispersion relation. These exceptionally synchronized modes of the structure become degenerate when a synchronized electron beam is coupled to the electromagnetic modes.

We define a “waveguide way” as an individual waveguide component (rectangular waveguide, SWG, etc.) which is not in cutoff over the designed operating frequency and can support two electromagnetic modes (one forward and one backward). A three-way waveguide supports six modes, when considering propagation in both the  $+z$  and  $-z$  directions, i.e., three modes in each direction. The three-way microstrip structure with SIP in [28] is what inspired the design of the structures in this paper.

The concept of “three-mode synchronization regime” using SIPs in the cold SWS dispersion of linear-beam tubes was initially proposed in [22] and was based on ideal transmission lines, following a multi-transmission line generalization of the Pierce model. Here, we show for the first time how one can design a realistic serpentine-like SWS to exhibit a cold SIP at millimeter-wave frequencies.

In Section II, we explain the concept of the SIP, smooth-TIP, and alternating-TIP. In Section III, we introduce the two proposed waveguide structures and we describe our design methodology to introduce SIPs in the three-way coupled waveguides. In Section IV, we show the dispersion, scattering parameters, and Pierce (interaction) impedance enhancement for our three-way coupled waveguides. All dimensions used in this paper are in SI units unless otherwise stated.

## II. COLD STATIONARY INFLECTION POINTS

Stationary inflection points are a special case of eigenmode degeneracy, whereby three eigenmodes coalesce at a single frequency point in the dispersion diagram for the modes of a periodic structure, as has been explored in [10], [12], [22], [32]–[40]. On the other hand, a *non-stationary*, or “tilted” inflection point is a single frequency point in the structure’s modal dispersion diagram where three eigenmodes are nearly coalescing, but not perfectly so. In the structure’s modal dispersion diagram, the dispersion relation local to an SIP or TIP will be cubic in shape. In general, these cubic-shaped dispersion relations will have an inflection point that occurs

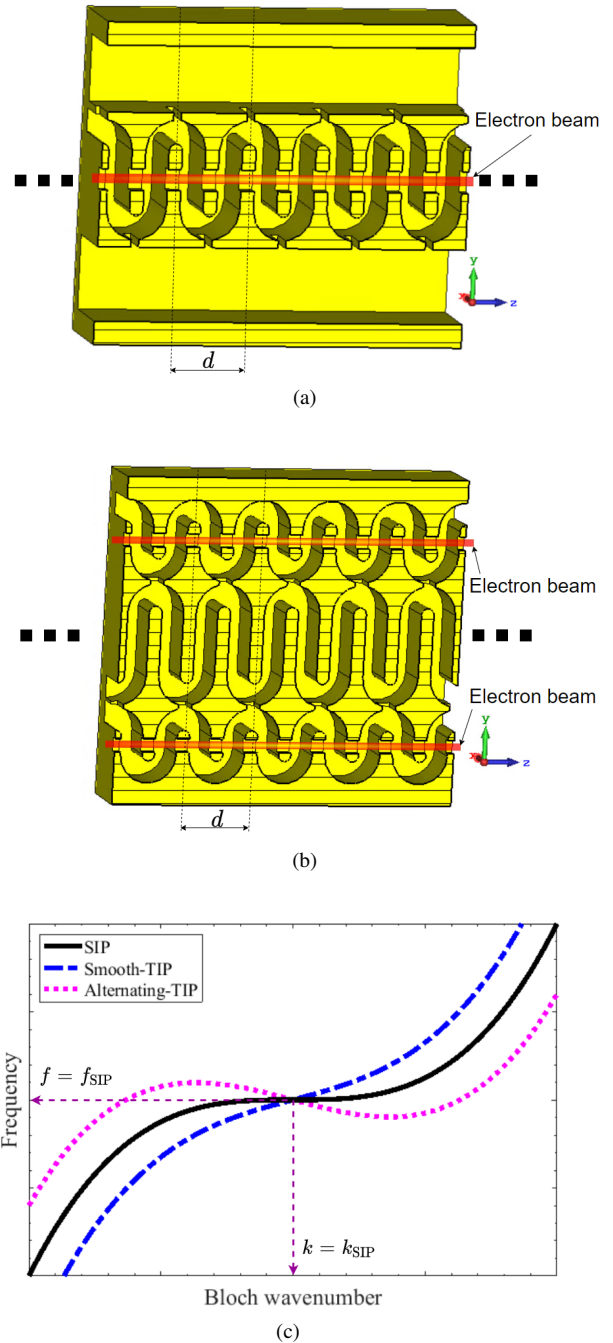


Fig. 1. Longitudinal cross-sections in the  $y$ - $z$  plane showing half of the periodic metallic structures composed by cascading (a) SLWG unit cells, and (b) TCSWG unit cells with periodicity  $d$ . Electron beams (red) are illustrated in beam tunnels. (c) Example of the dispersion relation of the mode with purely real wavenumber in the infinite periodic structure where the SIP occurs (black solid line) at a frequency  $f_{\text{SIP}}$  and fundamental wavenumber  $k_{\text{SIP}}$  where three modes coalesce (for clarity, only one mode is shown, the one with purely real wavenumber). The dispersion relation in the vicinity of an SIP is cubic. The three-way waveguide dimensions may also be slightly altered to make the SIP either a smooth-TIP (blue dash-dotted line) or alternating-TIP (magenta dotted line), rather than an SIP.

at a frequency-wavenumber combination where the second derivative of the  $\omega - k$  dispersion relation vanishes (i.e.  $d^2\omega/dk^2 = 0$ ). These inflection points are classified here into two kinds: the SIP, and the non-stationary inflection point, or TIP. The SIP occurs where both the first and second derivative of the  $\omega - k$  dispersion relation vanish at the same wavenumber, i.e.,  $d\omega/dk = 0$  and  $d^2\omega/dk^2 = 0$ . For the case of the TIP, only the second derivative of the  $\omega - k$  dispersion relation vanishes at the inflection point. In other words, the SIP is a special case of TIP. Because the modal dispersion diagrams for our lossless, reciprocal structures are symmetric in each Brillouin zone, the usual classification of non-stationary inflection points as rising or falling is ambiguous. Every reciprocal waveguide with a TIP in its dispersion relation will always exhibit two kinds of TIPs, rising and falling, for opposite signs of  $k_{\text{TIP}}$ . To remedy this, we further classify TIPs into two sub-categories: *smooth-TIPs* which have a non-vanishing group velocity that does not change sign for wavenumbers slightly above and below the inflection point, and *alternating-TIPs* which have a group velocity that alternates in sign as the wavenumber is swept near the inflection point, as illustrated in Fig. 1c.

We were able to design both the SLWG and TCSWG structures to exhibit SIPs in their cold dispersion, that is, without an electron beam present. We stress that this form of modal degeneracy is different from the hot eigenmode degeneracy, or “exceptional synchronization” studied in [29], [30]. The coalescence of the cold eigenmodes at an SIP results in a perfect cubic dispersion relation local to the SIP in the dispersion diagram,

$$(f - f_{\text{SIP}}) \simeq h(k - k_{\text{SIP}})^3. \quad (1)$$

When the cold eigenmodes of a structure are nearly-coalescing at a single wavenumber, and the dispersion relation exhibits a TIP, the dispersion relation local to the inflection point may be represented by a depressed cubic function (the quadratic term is suppressed due to the shift in  $k$  by the cubic function’s inflection point),

$$(f - f_{\text{TIP}}) \simeq h(k - k_{\text{TIP}})^3 + s(k - k_{\text{TIP}}). \quad (2)$$

The parameters  $f_{\text{SIP}} \simeq f_{\text{TIP}}$  and  $k_{\text{SIP}} \simeq k_{\text{TIP}}$  are the frequency and Floquet-Bloch wavenumber, respectively, at which the three eigenmodes coalesce or are nearly-coalescing to form an SIP or a TIP, respectively. We also note that, due to Floquet-Bloch spatial harmonics, the wavenumbers  $k$ ,  $k_{\text{TIP}}$ , and  $k_{\text{SIP}}$  in (1) and (2) have a periodicity of  $2\pi/d$ , where the pitch of the unit cell is  $d$ . That is,  $k$ ,  $k_{\text{TIP}}$ , and  $k_{\text{SIP}}$  in these formulae do not necessarily need to be within the fundamental Brillouin zone. The parameter  $h$  is a scalar flatness coefficient that depends on the strength of eigenmode coupling and  $s$  is a scalar coefficient that affects the “tilt” of the TIP, as demonstrated in Fig. 1c. Tilted inflection points and their properties, such as improved gain-bandwidth products and power efficiency, have also been explored in [22], using a multi-transmission line generalization of the Pierce model [41], [42].

At an SIP, the dispersion relation local to the inflection point is a cubic function similar to Eqn. (2) with  $s = 0$ , as shown in

solid black in Fig. 1c. At, and very close to, an SIP or smooth-TIP, the eigenwaves all propagate in the same direction. That is, the group velocities of the eigenwaves do not change sign at frequencies slightly lower and higher than  $f_{\text{TIP}}$ . At the inflection point of an SIP, the group velocity becomes zero. In a smooth-TIP with  $s > 0$ , the group velocity ( $d\omega/dk$ ) at the inflection point is no longer zero (blue dash-dotted line in Fig. 1c). Having the electron beam interact with an TIP with a near-zero positive group velocity (nearly-stationary TIP) instead of a perfectly-zero group velocity SIP may be preferable for TWT designs, since the Pierce (interaction) impedance at the frequency of the inflection point will be sufficiently large but the device will not become absolutely unstable when the electron beam is introduced. On the other hand, having an electron beam interact with a TIP that has negative group velocity is useful for the design of BWOs. We call this interaction between an electron beam and a cold SIP, a “three-mode synchronization” (see [22] for more details). Beamline interactions at points of zero group velocity, like the band-edge [43]–[46] or the degenerate band-edge (DBE) [17], [47], are to be avoided in the design of TWT amplifiers, as they are considered a source of instability. The alternating-TIP (magenta dotted line in Fig. 1c) is the second kind of TIP studied with  $s < 0$ , in which the group velocities of the eigenwaves will change sign at frequencies slightly lower and higher than  $f_{\text{TIP}}$ . If the geometry of a structure can be tuned to exhibit smooth-TIPs for one set of dimensions and alternating-TIPs for another set of dimensions, it is expected that such a structure can be made to exhibit an SIP.

From Pierce theory, the Pierce (interaction) impedance for a specific Floquet-Bloch spatial harmonic  $p$  and specific wavenumber corresponding to the frequency of interest is defined as

$$Z_{\text{Pierce}}(k_p) = \frac{|E_{z,p}(k)|^2}{2\text{Re}(k_p)^2 P(k)} \quad (3)$$

where,  $k_p = k + 2\pi p/d$  is the wavenumber corresponding to the appropriate  $p$ th Floquet-Bloch spatial harmonic,  $p = 0, \pm 1, \pm 2, \dots$ , and the wavenumber  $k$  is in the fundamental Brillouin zone defined here as  $kd/\pi \in [-1, 1]$ , i.e., with  $p = 0$ . Furthermore,  $|E_{z,p}(k)|$  is the magnitude of the phasor of the electric field component along the center of the beam tunnel in the  $z$  direction for a given wavenumber and  $p$ th Floquet-Bloch spatial harmonic, and  $P(k)$  is the time-average power flux at the fundamental wavenumber corresponding to the frequency of interest (the time average power flux is the sum of power contributions from all spatial harmonics) [48]. To obtain the magnitude of the axial electric field phasor, corresponding to the appropriate spatial harmonic, the complex axial electric field along the beam tunnel axis is decomposed into Floquet-Bloch spatial harmonics as  $E_z(z, k) = \sum_{p=-\infty}^{\infty} E_{z,p}(k) e^{-jk_p z}$ , where the harmonic weights are computed as  $E_{z,p}(k) = \frac{1}{d} \int_0^d E_z(z, k) e^{jk_p z} dz$  [49]. Both the complex axial electric field  $E_z(z, k)$  and the time-average power flux  $P(k)$  through the cross section of the unit cell are calculated for the cold structure (i.e. without the electron beam) using the eigenmode solver in CST Studio

Suite. However, one must pay careful attention to how the phase across the periodic boundaries is defined in the CST model to correctly compute the interaction impedance. Since the  $\exp(j\omega t)$  time convention is used by CST, the formula for calculating  $E_{z,p}(k)$  requires a delaying phase from the lower periodic boundary to the upper periodic boundary of the simulated unit cell, i.e. phase of  $E_z(z, k)$  must decrease from  $z_{min}$  to  $z_{max} = z_{min} + d$  for a positive value of  $k$ . Conveniently, the electromagnetic energy simulated within the enclosed vacuum space of the unit cell between periodic boundaries in the eigenmode solver, which is based on the finite element method (FEM) implemented in the software CST Studio Suite, is always assumed to be 1 Joule for each eigenmode solution. Therefore, the power flux is calculated using the formula  $P = (1 \text{ Joule})v_g/d$ , where  $d$  is the unit cell pitch, and the group velocity  $v_g = d\omega/dk$  is determined directly from the dispersion diagram via numerical differentiation (The group velocity is the same at every spatial harmonic).

In order for interaction impedance to be large, the ratio in Eqn. (3),  $|E_{z,p}(k)|^2/P(k)$ , must become large in magnitude or the wavenumber in the denominator must become very small (i.e., operating closer to the fundamental spatial harmonic). At a nearly-stationary TIP, which is close to becoming an SIP, the power flow at the inflection point is indeed smaller than the power flow of conventional SWG at the same wavenumber of the inflection point, this because the power flow is proportional to the group velocity. Assuming that the magnitude of the axial electric field component is comparable for both cases, one concludes that the Pierce impedance will be larger for the structure with an inflection point than in a conventional SWG, at the wavenumber corresponding to the inflection point.

Due to this phenomena, it is possible to obtain a moderately high, narrowband Pierce impedance at an SIP or nearly-stationary TIP, which is several times larger than the Pierce impedance observed in a conventional serpentine waveguide, as demonstrated in Sec. IV.

Conventional TWT SWS exhibit higher symmetries, such as glide symmetry in the serpentine-type TWT or screw symmetry in the helix-type TWT [50], [51]. Nearly parallel dispersion curves are formed by breaking glide symmetry. Glide symmetry can be broken in our structures by introducing minor dimensional differences between two similar waveguide sections. This allows us to readily tune the tilt of TIPs in our dispersion relation by simply varying one or more of our structure's dimensions.

Next, we show the design methodology for two kinds of SWS geometries, whose unit cells are shown in in Fig. 2, that can be dispersion engineered to exhibit SIPs or nearly-stationary TIPs.

### III. PROPOSED WAVEGUIDES EXHIBITING SIP

#### A. Serpentine Ladder Waveguide (SLWG)

The SLWG was our first attempt at obtaining a SWG-like structure which is capable of exhibiting an SIP and has its geometry shown in Fig. 2a. As we will show in our dispersion diagrams in Section IV, the SLWG structure can be potentially designed to operate as a BWO due to the backward

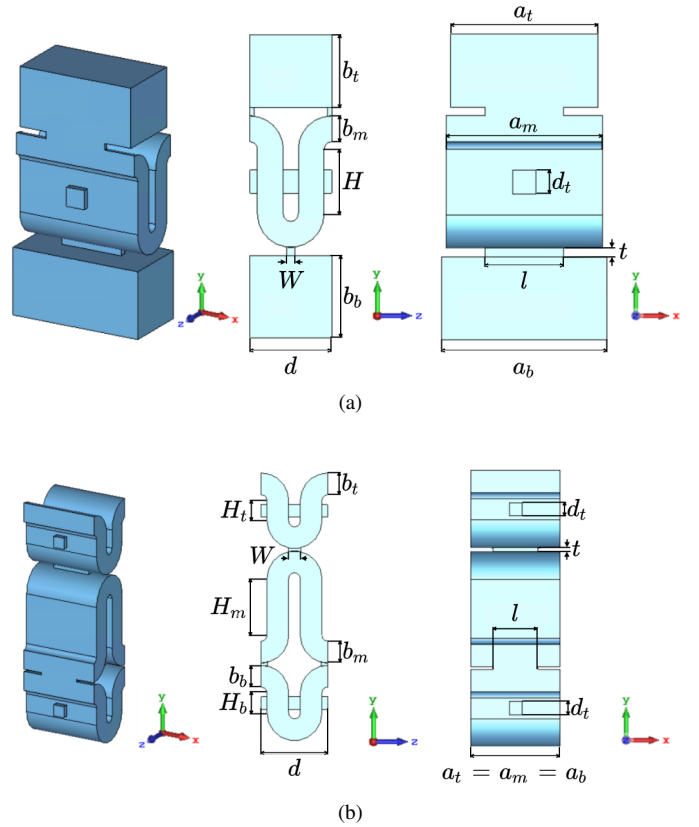


Fig. 2. The two unit cell geometries of the two three-way waveguides studied in this paper. The unit cells are constructed by periodically coupling three waveguides. Only the vacuum space inside the waveguides is shown (i.e., no metallic walls are shown). (a) SLWG unit cell with one square beam tunnel threaded through the middle SWG. The middle SWG is coupled to two lateral straight waveguides with larger waveguide heights ( $b$  dimension) than the middle SWG, (b) Dual-beam TCSWG unit cell with square beam tunnels threaded through top and bottom SWGs. Background material is PEC. Waveguide ways have subscripts  $t$ ,  $m$ , and  $b$  (top, middle, and bottom) based on their relative positions along the  $y$ -axis. Rectangular coupling slots which are in cutoff are added between middle SWG bends and adjacent waveguide ways.

waves that are exhibited where the beamline interacts with an SIP or smooth-TIP. This behavior is also illustrated by the intersection of the inflection point (solid brown curve) and the beamline (dashed red line) in the dispersion diagram of Fig. 3a. Furthermore, since the guided electromagnetic modes of the SLWG structure are distributed over a larger cross section than a conventional SWG due to the two lateral waveguides that couple to the middle SWG, the power handling capability of this structure may be enhanced. The SLWG structure is a serpentine waveguide SWS which is sandwiched between two straight, parallel rectangular waveguides with similar broad wall dimensions. A single beam tunnel is through the center of the SWG structure. The structure resembles a ladder due to the rung-like appearance of transverse serpentine sections running between the parallel straight waveguides. The parallel waveguides are each weakly coupled periodically to the SWG at the middle of each bend by small rectangular slots, as shown in the longitudinal cross section of Fig. 1a and in the dimensional markup of the unit cell, Fig. 2a. This waveguide structure was inspired by a similar microstrip three-

way periodic structure which also exhibits SIPs [28]. However, our structures are only able to exhibit SIPs in the fundamental  $TE_{10}$  rectangular waveguide mode by breaking glide symmetry at this time.

The dispersion curves corresponding to the  $TE_{10}$  mode of the individual parallel rectangular waveguides must be bent and vertically shifted in order to obtain an SIP or TIP of a desired tilt and frequency in the SLWG dispersion relation, as will be further described in Sec. III-C.

Introducing small dimensional differences between the top and bottom parallel waveguide ways (i.e., changing the broad wall dimensions  $a_t$  and  $a_b$  as shown in Fig. 2a) or introducing metallic obstacles of different dimensions in the top and bottom parallel waveguides breaks glide symmetry. Breaking glide-symmetry provides a simple route to achieve a cold SIP in the structure's dispersion relation once periodic coupling is introduced between individual-waveguide modes. These differences between the top and bottom waveguides directly control the tilt of the TIP. In general, breaking glide symmetry is not a necessary condition to have an SIP, as three-way waveguide structures with unbroken glide-symmetry have been previously shown to exhibit SIPs [28]. However, here it has been found to be convenient to achieve and manipulate SIPs in structures with broken glide-symmetry, as the SIP can occur within the fundamental  $TE_{10}$  mode of the SWG below upper band-edge associated to the bandgap of the SWG which occurs at  $k = 2\pi p/d$ .

### B. Three Coupled Serpentine Waveguide (TCSWG)

The three-coupled serpentine waveguide TCSWG structure is our second example of a serpentine-type SWS that is capable of exhibiting SIPs in its dispersion relation, and has its geometry shown in Fig. 2b. The TCSWG seems to be better suited for use in a TWT than the SLWG structure, since the example we show tends to exhibit forward waves in proximity to the synchronization point where the beamline interacts with an SIP or a smooth-TIP, as we will show in our dispersion diagrams in Section IV. The TCSWG structure is constructed similarly to the SLWG structure. However, the top and bottom rectangular waveguides which sandwich the center SWG are also made to be serpentine in shape, giving them a longer path length and similar dispersion shape to that of the center SWG, as shown in the longitudinal cross-section of Fig. 1b and in the dimensional markup of the unit cell in Fig. 2b. No periodic obstacles or broad wall dimension variations are required, as the mean path lengths of each individual waveguide way may be altered to break glide-symmetry and obtain an SIP. In our TCSWG structure, the top, bottom, and middle SWGs each have the same pitch and broad wall dimension. The straight section height of each SWG way ( $H_t$ ,  $H_m$ ,  $H_b$ ) is varied to alter the shape of its respective dispersion curve, allowing the prementioned SIP conditions to occur. The tilt of the TIP is controlled by the size of the coupling slots placed between bends of adjacent SWSs, as well as minor path length differences (between the serpentine height dimensions  $H_t$  and  $H_b$ ) introduced to break glide symmetry. We have also found that if the path length of the middle SWG, mainly controlled

by  $H_m$ , is made to be a scalar multiple of the top or bottom path length that is greater than two, it is possible to have multiple SIPs or TIPs in synchronism with the beamline at different frequencies, though we do not show it in this paper.

Instead of inserting a beam tunnel only in the center SWG, it is also possible to add beam tunnels to the center of the top and bottom SWGs. This makes the structure operate with two beams propagating parallel to each other, provided that the two beams are not too close together and an external magnetic field can be used to confine both beams. This dual-beam structure can potentially benefit from increased power output at the SIP/TIP due to beamline synchronism in both the top and bottom SWG sections.

### C. Design methodology

A minimum of three ways is required to obtain an SIP in a reciprocal, lossless, cold structure. This is because the SIP is a synchronous coalescence of three eigenmodes. In order to design three-way serpentine waveguide SWSs that are both consistently synchronized to a beamline and exhibit SIPs, we utilize a design methodology based on the work of [52]. We use a dispersion approximation for the initial design of both the individual straight rectangular waveguide and serpentine waveguide ways. The design process begins by selecting a fixed center operating frequency, spatial harmonic number  $p$ , cell pitch  $d$ , and average electron beam velocity  $u_0$  determined from the cathode-anode voltage of an electron gun. The full-cell pitch  $d$  in our work is chosen to be equal to  $\lambda_g/4$ , where  $\lambda_g = 2\pi / \left( k_0 \sqrt{1 - c/(2af_{center})^2} \right)$  is the guided wavelength at the center operating frequency within the SWG containing the beam tunnel, where  $k_0$  is the free space wavenumber,  $c$  is the velocity of light in free space,  $a$  is the broad-wall dimension of the individual waveguide cross-section as shown in Fig. 2, and  $f_{center}$  is the center operating frequency.

Starting with the average beam velocity,  $u_0$ , the beamline's linear relation (neglecting space charge effects) between the frequency and average electronic phase constant,  $\beta_0$ , is

$$\beta_0 = \frac{2\pi f}{u_0}. \quad (4)$$

Then, the dispersion for the  $p^{th}$  spatial harmonics of the individual serpentine and/or straight waveguide sections is calculated from the relation found in [52]

$$f = f_c \sqrt{1 + \left( \frac{a}{L} \right)^2 \left( \frac{kd}{\pi} - 2p \right)^2}, \quad (5)$$

where,  $f_c = c/(2a)$  is the cutoff frequency of the rectangular waveguide cross-section and  $L = 2H + \pi d/2$  is the mean path length of the individual uncoupled waveguide section within the unit cell, as can be observed in the serpentine waveguide sections of Fig. 2. To model the dispersion of a straight rectangular waveguide sections of Fig. 2a, the path length simply becomes equal to the pitch of the unit cell,  $L = d$ . We describe our structure using a full unit cell notation (of period  $d$ ) rather than the half unit cell notation (of period  $d/2$ ) commonly used in literature. The half-cell notation is often used because the beam "sees" two beam tunnel intersections

per geometric period of the full unit cell, which only differ by a sense-inversion of  $E_z$  fields at each consecutive beam tunnel intersection. The primary difference is that the path lengths of each individual waveguide of our full unit cell are twice as long as they would be in the half-cell notation. Much of the fundamental spatial harmonic of the full-cell dispersion diagram lies above the light-line of  $k_0 = \pm\omega\sqrt{\mu_0\epsilon_0}$  and cannot be utilized for amplification without the use of a relativistic beam velocity [2]. Because the full-cell notation is being used in this paper rather than the half-cell notation, the additional  $\pi$  phase shift considered in some other papers such as [52]–[55] is no longer needed, so the term  $2p + 1$  in [52] has been replaced with  $2p$  in (5). As long as the coupling between waveguide sections in each unit cell is weak, this dispersion relation will serve as a reasonably accurate approximation of actual dispersion below the first  $k = 2\pi p/d$  bandgap, which occurs at the intersection of two neighboring spatial harmonic curves corresponding to the same individual waveguide way which contains the beam tunnel.

The dimensions  $a$  and  $H$  of the SWG sections containing beam tunnels, as shown in Fig. 2, are selected using an optimization algorithm which minimizes the integrated frequency error between the beamline and SWG dispersion curves over the wavenumber interval of  $kd/\pi \in [2p, 2(p+1)]$ . This wavenumber interval corresponds to the frequency range over which amplification is desired to occur in our paper, as shown in Fig. 3a and Fig. 3b. Once suitable  $a$  and  $H$  dimensions are determined for the SWG with a beam tunnel, the narrow wall  $b$  dimension of our serpentine waveguide way was chosen to be  $b = a/6$  to provide adequate spacing between the SWG beam tunnel intersections. Of course, in most SWG structures, the  $a$  and  $b$  dimensions are rarely close to standard waveguide sizes due to the need for synchronism with a specific beamline, so waveguide transitions are needed at the input and output ports to allow connections for standard waveguide sizes, in addition to radio frequency (RF) windows to maintain vacuum within the tube. However, for simplicity, we do not consider such waveguide transitions or windows in our study, and we only focus on the beam-wave interaction region. The beam tunnel diameter  $d_t$  is selected based on the empirical formula from [52],

$$d_t = L\alpha \left( 1 + \left( \frac{L}{2a} \right)^2 \right)^{-\frac{1}{2}}, \quad (6)$$

which minimizes the width of the bandgap caused by the beam tunnel. The ratio of the beam tunnel radius to the free space wavelength at the  $2\pi$  frequency,  $\alpha \simeq 0.115$ , was used in the design of our structures as well. The bandgap normally caused by the beam tunnel is significantly widened due to the additional periodic reactive loading introduced by coupling slots. Increasing the size of the coupling slots introduces stronger coupling between the waveguide sections, but enlarges the bandgap. Therefore, simply having a beam tunnel which is sufficiently in cutoff appears to be adequate for these kinds of structures. A square-shaped beam tunnel with side length  $d_t$  may also be used in place of a conventional cylindrical beam tunnel, as shown in Fig. 2, to make the structures more compatible with multi-step LIGA (lithogra-

phie, galvanofornung, abformung; German for lithography, electroplating, and molding) processes [56]. Traveling wave tube amplifiers with square beam tunnels may be fabricated using two-step LIGA processes like in [57]–[63]. In the two-step LIGA process, the SWSs are electroformed out of two symmetric halves which are later bonded together. However, more than two steps will likely be necessary for our structures due to the coupling slot lengths differing from the beam tunnel width or differing broad wall dimensions in each waveguide way. Additionally, the use of a square beam tunnel may slightly degrade the hot operation of TWTs, as mentioned in [60], [61], [64]. While it is potentially challenging to fabricate such structures using LIGA fabrication, it should not be significantly more challenging than it already is for conventional serpentine waveguides fabricated by two-step LIGA. For example, each additional LIGA step required for the SLWG and TCSWG structures corresponds to a repetition of procedures 7-13 (lapping/polishing, photoresist attachment, mask,  $n^{\text{th}}$  layer alignment, exposure, development, and electroplating) after procedure 13 shown in [61].

The dispersion condition of the waveguides (when uncoupled to each other) utilized by our group to consistently obtain SIPs is to have two nearly parallel uncoupled (individual-waveguide) modes cross over a third (individual-waveguide) mode which is nearly perpendicular to the other two modes on the dispersion diagram, as shown in Fig. 3. If a periodic coupling is introduced between all three of the individual-waveguide modes and the nearly parallel individual-waveguide modes are in close proximity in the dispersion diagram, then two phase- and frequency-shifted bandgaps will form at the intersection points. If the top band-edge of one bandgap tangentially touches the bottom band-edge of another bandgap, an inflection point is able to form between these band-edges, as illustrated in the inset of Fig. 3a and Fig. 3b. Varying the proximity of near-parallel individual-waveguide modes for a given coupling strength directly controls the tilt of the TIP. Near-parallel individual-waveguide modes which are close to each other tend to form smooth-TIPs, whereas near-parallel individual-waveguide modes which are further from each other will typically form alternating-TIPs. Between smooth-TIP and alternating-TIP conditions, an SIP condition is expected to exist.

Once the basic dimensions of the SWGs with beam tunnels are established, coupling slots are positioned between the bends of adjacent waveguide ways to periodically couple the individual-waveguide modes. The coupling slots have a vertical thickness  $t$  in the  $y$ -direction, width  $w$  in the  $z$ -direction, and length  $l$  in the  $x$ -direction, as shown in Fig. 2. The length of the coupling slot, which is also along same axis as the broad wall dimension of the waveguide ways, is the dimension that strongly controls the evanescent coupling of modes between waveguide ways. The width of the coupling slot controls the wave impedance within the slot, and the slot thickness primarily controls the extent of evanescent decay and phase delay for waves which are below the slot cutoff frequency. In this paper, we use a coupling slot length equal to half the  $a$  dimension of the SWG section containing the beam tunnel. The slot width and thickness are arbitrarily chosen in



this paper to demonstrate that SIPs can be attained in our structures. Larger slot lengths will strengthen mode coupling, but the dispersion relation of the actual structure will be strongly dissimilar to the dispersion relation of the individual uncoupled waveguide modes from before. While large slot lengths and widths enhance mode coupling, the reflections introduced by the periodic slot reactance in a finite-length structure may also make the hot structure more susceptible to regenerative oscillations.

Finally, a small geometric difference is introduced between the waveguide sections corresponding to near-parallel dispersion curves to control the frequency and wavenumber spacing between near-parallel dispersion curves. This directly controls the tilt of the TIP. Large geometric differences typically result in an alternating-TIP, whereas small geometric differences make the TIP smooth. For the TCSWG structure, geometric differences may be introduced as a height difference  $\Delta H = |H_t - H_b|$  between the top and bottom serpentine sections ( $H_t$  and  $H_b$  in Fig. 2b, respectively). For the SLWG structure, a broad wall dimension difference  $\Delta a = |a_t - a_b|$  may be introduced between the top and bottom straight waveguide sections ( $a_t$  and  $a_b$  in Fig. 2a, respectively). Alternatively, geometric differences may be introduced in periodic capacitive obstacles loading the top and bottom straight waveguides of the SLWG structure to achieve the same effect, reducing the number of steps required for LIGA fabrication. However, it may not be desirable to use periodic obstacles due to the large reflections they introduce in the top and bottom waveguide sections of the SLWG structure. Conversely, the use of unloaded parallel waveguides also reduces the complexity and reflection coefficients of SWS at the cost of more steps with LIGA fabrication.

Once all initial structure dimensions are determined, the full unit cell geometry may be simulated in an eigenmode solver to obtain the Pierce (interaction) impedance and  $\omega - k$  dispersion relation with real-valued wavenumber,  $k$ . In this paper, we use the software CST Studio Suite to obtain the modal dispersion for each periodic structure. Using simulated dispersion data, the  $a$  and  $H$  dimensions of SWG ways containing beam tunnels are then further tuned to recover beamline synchronism. Adjusting the  $a$  dimensions of each serpentine waveguide shown in Fig. 2a ( $a_m$ , for the middle SWG of the SLWG structure;  $a_t$  and  $a_b$  for the top and bottom SWGs of the TCSWG structure) primarily serves to shift each respective SWG dispersion curve up or down. Adjusting the  $H$  dimension primarily controls the slope of the SWG dispersion curve, which may have changed due to periodic loading from the slots. When the modal dispersion curves and TIP are satisfactorily synchronized to the beamline, the geometric difference between waveguide sections corresponding to parallel dispersion curves (for example,  $\Delta a$  in the SLWG structure or  $\Delta H$  in the TCSWG structure) may then be tuned to adjust the tilt of the TIP to make it close to an SIP.

#### IV. RESULTS

Following the aforementioned design procedures of the previous section, we obtain the real part of the modal dispersion

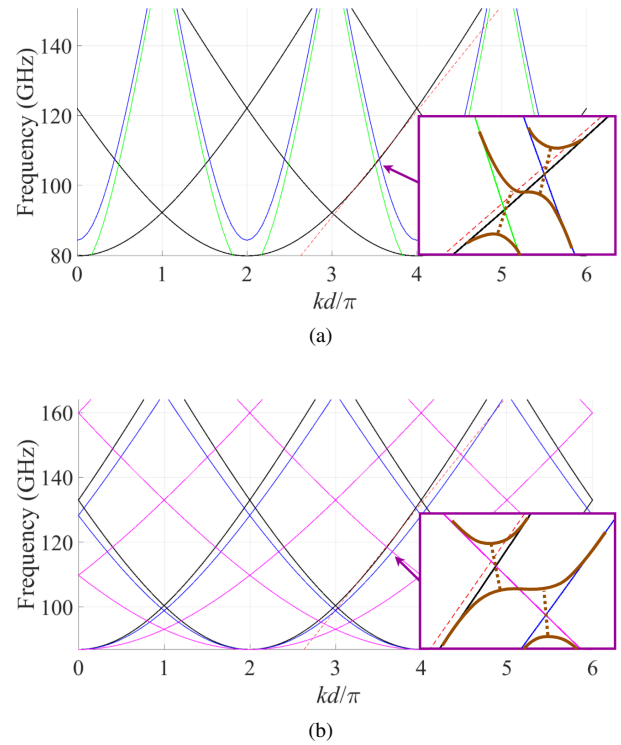


Fig. 3. Dispersion for the individual (uncoupled) waveguides in (a) SLWG structure with a small difference between the broad-wall widths of top and bottom waveguides  $\Delta a = |a_t - a_b|$  (blue and green curves for the straight waveguides, black for the SWG, and dashed red curve for the beamline) and (b) TCSWG structure with a small difference between serpentine heights of top and bottom SWGs  $\Delta H = |H_t - H_b|$  (blue and black curves for the top and bottom SWGs, magenta for the center SWG, and dashed thin red curve for the beamline). Each solid curve corresponds to the dispersion of an individual-waveguide way based on Eqn. 5. The width and cutoff frequency of each dispersion curve can be set by adjusting the corresponding geometry for the individual-waveguide way. Insets of figures (a) and (b) illustrate SIP formation when coupling is introduced (thick brown curves, dotted brown lines for tilted bandgaps). Introducing coupling between the waveguides causes bandgaps to form at each dispersion curve intersection. If two nearly-parallel individual-waveguide dispersion curves cross over a third individual-waveguide dispersion curve, it is possible to obtain an SIP. The SIP or TIP occurs where the lower band-edge of one bandgap meets the upper band-edge of an adjacent bandgap. Tilted inflection point “tilt” may be adjusted by varying coupling strength or by adjusting the distance between parallel individual-waveguide dispersion curves. Dimensions for this example are provided in Appendix A.

relation (for the lossless and cold structures shown, imaginary parts of the dispersion relation correspond to evanescent modes, e.g. below the cutoff frequency of the waveguide or in bandgaps where neighboring spatial harmonics meet on the dispersion diagram) for both SLWG and two-beam TCSWG structures, as shown in Figs. 4a and 4b, obtained using the methods shown in Appendix B and verified using the eigenmode solver in CST Studio Suite. In the insets of these figures, we also demonstrate how it is possible to vary the tilt of the inflection point for three different cases simply by altering the difference in straight waveguide widths ( $a_t$  and  $a_b$  for top and bottom rectangular waveguides, respectively) for the SLWG structure, or the serpentine waveguide heights ( $H_t$  and  $H_b$ ) of the top and bottom waveguides. The dimensions of each case are provided in Appendix A. From the dispersion relation shown for the SLWG in Fig. 4a, the point where

the beamline intersects an SIP or smooth-TIP (solid black and dashed blue curves, respectively) is a backward-wave interaction, making the SLWG design better suited for use in a BWO rather than a TWT. While an alternating TIP (magenta dotted curve in the inset of Fig. 4a) might enable forward-wave interactions in the SLWG structure, the upper and lower band-edges on either side of the inflection point still pose a significant risk for oscillations. Backward wave oscillators constructed with the SLWG structure may also benefit from improved power handling capability compared to a conventional SWG BWO due to the guided electromagnetic mode being distributed over a larger cross section in the two lateral waveguides.

From the dispersion relation for the TCSWG structure in Fig. 4b, the point where the beamline intersects the inflection point is a forward wave for the SIP and smooth-TIP (solid black and dashed blue curves, respectively), making the TCSWG structure a better choice for TWT designs. While the TCSWG structure shown is designed for velocity-synchronism with an electron beam at the inflection point, which is inherently a narrowband phenomenon, this does not mean that the bandwidth of TWTs built using the TCSWG structure is severely limited. Because we initially designed these structures with broadband beam-wave synchronization in mind, there are still broad frequency ranges along dispersion branches above and below the designed inflection points, where the beamline is velocity-synchronized to the guided waves. It is still possible to amplify waves over broad bandwidths as long as the TWT is stable when the beam is introduced.

Additionally, metal losses and manufacturing errors may perturb the dispersion relation of an SIP or TIP from its intended design, so such effects need to be considered in the fabrication and testing of SLWG and TCSWG structures. Waveguide structures exhibiting EPDs are known to be quite sensitive to losses and fabrication tolerances [23], [26]–[28]. For the example SLWG structure in this paper, the geometric difference in  $\Delta a$  needed to go from an SIP to a smooth/alternating TIP in the inset of Fig. 4a is  $30 \mu\text{m}$ . For the example TCSWG structure, a difference in  $\Delta H$  of  $50 \mu\text{m}$  is needed to go from an SIP to a smooth/alternating TIP in the inset of Fig. 4b. The work of Li, *et al.* [58] shows that it is possible to fabricate serpentine waveguide structures with  $6 \mu\text{m}$  depth tolerance (for the broad-wall dimension  $a$  of our structures) and  $2 \mu\text{m}$  width tolerance between sidewalls using ultraviolet LIGA (UV-LIGA) fabrication techniques. A fabrication tolerance of  $6 \mu\text{m}$  (20% of the difference in  $\Delta a$  needed to go from an SIP to a smooth/alternating TIP shown in Fig. 4a for the SLWG structure) is acceptable to obtain a SLWG structure that exhibits a nearly-stationary inflection point. For the TCSWG structure, a tolerance of  $2 \mu\text{m}$  for sidewall widths (4% of the difference in  $\Delta H$  needed to go from an SIP to a smooth/alternating TIP shown in Fig. 4b for the TCSWG structure) is even better. Though, of course, these tolerances may be relaxed for designs that have an SIP/TIP at lower frequencies.

Due to the neighboring upper and lower band edges in proximity to the inflection point, one must also carefully “aim” the beamline, which is directly controlled by the accelerating volt-

age of the electron gun, to avoid striking dispersion branches that have zero group velocity, such as the band edge, as it can lead to instability [43]–[46]. Because there are upper and lower band edges at frequencies close to the inflection point, the tuneability of the beam voltage is limited. For instance, in Fig. 4a, neglecting space charge (i.e. at low beam currents), the average beam velocity can only be varied by approximately  $u_0 = 0.200c \pm 0.001c$  to avoid striking the neighboring upper or lower band edges on other dispersion branches. This beam velocity range corresponds to an approximate kinetic equivalent voltage tuneable range of  $V_0 = 10.54 \pm 0.11 \text{ kV}$  from the relativistic relation  $V_0 = c^2/\eta \left[1 - (u_0/c)^2\right]^{-1/2}$  in [65], where  $\eta$  is the charge-to-mass ratio of an electron at rest. For the case of the TCSWG structure we show, the tuneable range of the beam velocity equivalent kinetic voltage is better due to the neighbouring upper/lower band edges near the inflection point being separated at higher/lower frequencies, respectively, as can be observed in Fig. 4b. However, there is still a risk of oscillations at the lower band edge corresponding to a frequency of approx. 133 GHz for the structure shown, so the tuneable range of beam velocity for the TCSWG structure is  $u_0 = 0.300c \pm 0.002c$ , which corresponds to an approximate beam voltage range of  $V_0 = 24.67 \pm 0.36 \text{ kV}$ .

One must also consider how the electron beam perturbs the inflection point in the hot dispersion relation for the three-mode synchronization regime, as was explained in [22]. When an electron beam is introduced to the system, the SIP or TIP which existed in the cold dispersion relation will be deformed in the hot dispersion relation. The amount that the electron beam perturbs the inflection point depends primarily on the dc beam current density, with higher currents causing larger perturbations to the inflection point in the hot dispersion relation.

Similar to other three-way waveguide power dividers and combiners explored in papers such as [66]–[68], our structures also exhibit directional coupler-like behavior at its SIP/TIP frequencies, as demonstrated with a finite-length structure of 32 unit cells, shown in Figs. 5a and 5b. The S parameters of the finite length structure were calculated using the methods explained in Appendix B. The port numbering scheme for our structures is that the input ports at the electron-gun end of the structure (on the left) are odd-numbered from top to bottom, and output ports at the collector end of our structure (on the right) are even-numbered from top to bottom. While it is highly important to consider the effect of waveguide transitions and RF windows, our study focuses primarily on the interaction region of linear beam tubes, so for brevity we do not consider the effect of input/output coupling structures; i.e. we only consider the S-parameters at reference planes between the SWS and where an RF window would be placed in a fabricated device. This directional coupler-like behavior enables distributed power extraction (DPE) which can be directed either backward toward the cathode-end of the structure or forward toward the collector-end of the structure. However, only forward-directive DPE may be desired for amplification, due to the potential risk of regenerative oscillations introduced by amplified waves returning to the electron gun-end of the



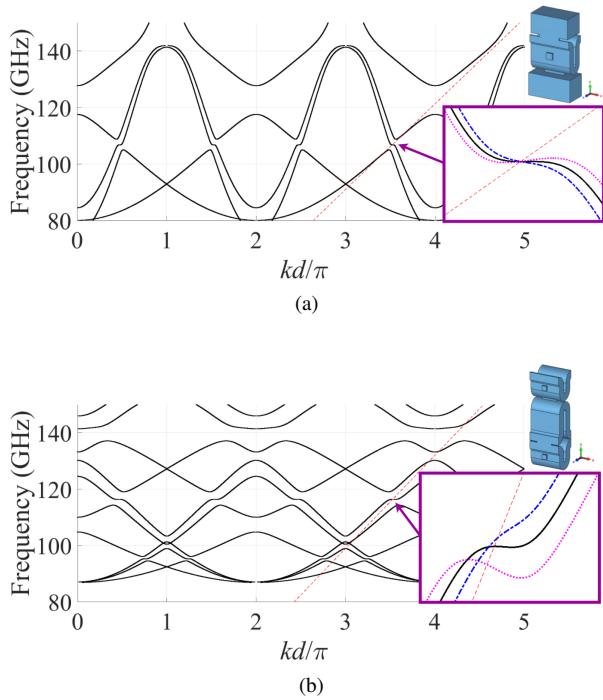


Fig. 4. Modal dispersion diagrams for (a) SLWG unit cell, and (b) TC-SWG unit cell, with beamline (red dashed). The insets show a smooth-TIP, alternating-TIP, and SIP in blue (dashed line), magenta (dotted line), and black (solid line), respectively for each structure. Only wavenumbers which are purely real are shown. The dispersion diagrams in the figure are obtained using the methods shown in Appendix B, and the dispersion relations were verified using the full-wave eigenmode solver of CST Studio Suite. Tilting of the inflection point is achieved by fine-tuning one or more of the structure dimensions. Dimensions for the smooth-TIP, alternating-TIP, and SIP are available in Appendix A.

structure, like in [69]. The introduction of distributed power extraction for linear beam tubes was necessary to conceive the degenerate (or exceptional) synchronization in the hot systems studied in [29]–[31]. For the TCSWG structure, increasing the path length of the middle SWG can allow forward-directive DPE to occur at certain frequencies and for power to be extracted in the top, middle, and bottom SWG outputs. However, there may still be SIP/TIP frequencies where backward-directive DPE continues to occur. Shifting the frequency above or below the SIP/TIP in the vicinity of the inflection point directly controls whether the top or bottom SWG section contributes more power to the output of the middle SWG, as can be seen from the scattering parameters. This dual beam TCSWG structure may also be excited either from the middle SWG input or top and bottom SWG inputs to achieve amplification and DPE at the SIP/TIP frequency if coupling is sufficient. Increasing the size of coupling slots enhances DPE, however this also exacerbates reflections in the finite-length structure and increases risk of BWO. Because these structures can still be designed to be well-matched with small coupling slots, longer finite-length structures and higher beam currents may potentially be used before unstable BWO occurs in PIC simulations and hot testing.

Finally, we compute the Pierce impedance as discussed in Section II for a fourth case of the SLWG structure in the vicinity of a nearly-stationary smooth-TIP, which has

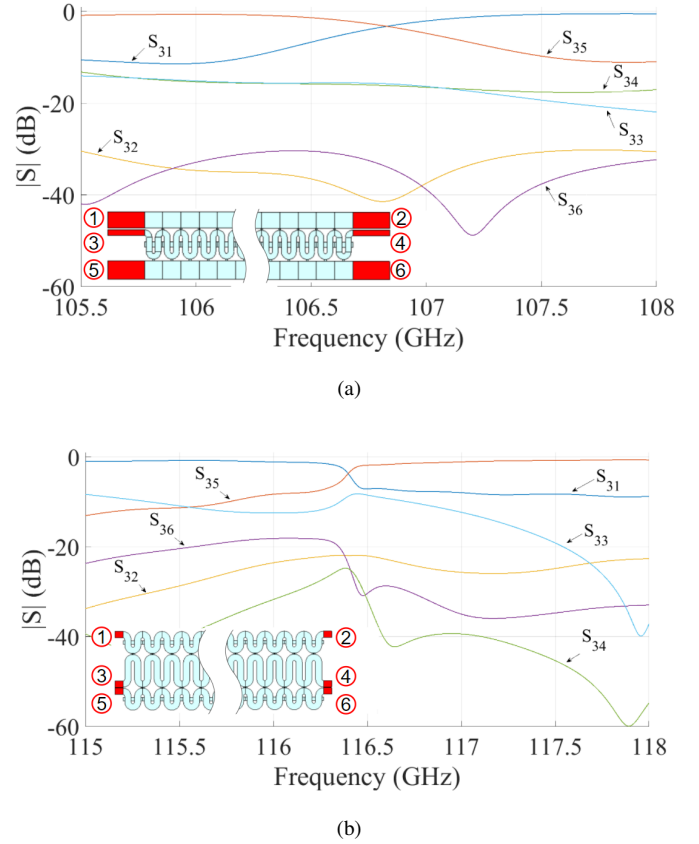


Fig. 5. SWS with 32 unit cells and S parameters for (a) SLWG and (b) TCSWG in the vicinity of the SIP with port numbering scheme. Port de-embedding is shown in red. Scattering parameters are calculated using the method explained in Appendix B.

dispersion relation similar to the black curve, but the inflection point is not as tilted as the blue curve, shown in Fig. 4a, with dimensions provided in Appendix A. We demonstrate the benefit of using nearly-stationary TIPs to enhance the Pierce impedance of serpentine-like structures, as shown in Fig. 6. We also compare the Pierce impedance of the SLWG (solid blue line) to the Pierce impedance of a conventional individual SWG (red dotted line) (i.e., the serpentine of the SLWG structure, with removed coupling slots and straight waveguide ways). We find that the pierce impedance of the full SLWG structure is several times higher than a conventional simple serpentine waveguide at the frequency corresponding to a nearly-stationary inflection point. We also note that, while the interaction impedance of the SLWG appears quite small relative to the simple SWG at frequencies beyond the inflection point, the interaction impedance is comparable that of an SWG on other higher/lower frequency branches of the SLWG's dispersion diagram, which are not shown.

Similarly, we compute the Pierce impedance for the a fourth case of the dual-beam TCSWG structure in the vicinity of the nearly-stationary smooth-TIP, which has a dispersion similar to the black curve, but not as tilted as the blue curve shown in the inset of Fig. 4b, with dimensions provided in Appendix A. We demonstrate that the nearly-stationary TIP can be used to enhance the Pierce impedance in both beam tunnels, as shown

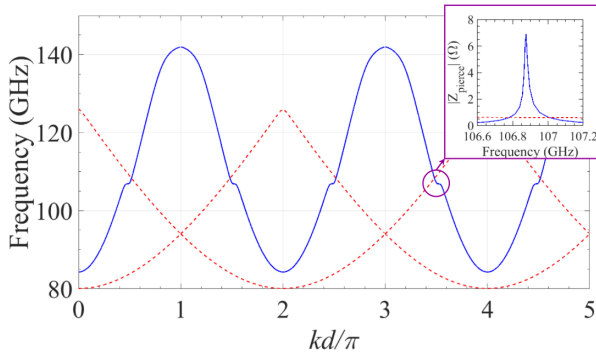


Fig. 6. Pierce (interaction) impedance (solid blue curve in inset) for the SLWG calculated from the field along the beam tunnel for the eigenmode with a TIP, associated to the circled region in the dispersion diagram (solid blue curve in main figure). Nearly-stationary TIP with negative fundamental  $k$  (i.e., in the fundamental Brillouin zone defined here as  $kd/\pi \in [-1, 1]$ ) is circled for the  $p = 2$  spatial harmonic. The Pierce impedance at the TIP is compared to the Pierce impedance associated with the eigenmode of an individual serpentine waveguide with coupling slots and straight waveguide geometries removed (red dashed). Specifically, the Pierce impedance was evaluated over the phase interval  $kd/\pi \in [-0.53, -0.43]$  for the TIP at the appropriate spatial harmonic  $p = 2$ . The dispersion diagram of the individual SWG mode (dashed red) is also shown in the main figure. The dispersion curves in the main figure were found using the eigenmode solver of CST Studio Suite.

in Fig. 7. We compare the Pierce impedance of the TCSWG structure (solid blue line) to the Pierce impedance of a conventional individual SWG (i.e. with coupling slots and adjacent waveguide sections removed) for each respective beam tunnel (dashed red for the top SWG, dotted magenta for the bottom SWG). We find that, just like with the SLWG structure, the Pierce impedance is several times higher than a conventional SWG at the frequency corresponding to the nearly-stationary inflection point. Interestingly, below the frequency of the TIP, the interaction impedance in the lower beam tunnel is higher than in the upper beam tunnel, whereas the opposite occurs at frequencies above the TIP. Since glide symmetry is slightly broken due to the top and bottom SWGs having different  $H_t$  and  $H_b$  dimensions, respectively, the dispersion branches of the individual SWGs (red dashed line for the top SWG and magenta dotted line for the bottom SWG) are dissimilar. Due to broken glide symmetry, the peak values of interaction impedance in the top and bottom tunnels are also different at the inflection point. If an electron beam is introduced to the SLWG or TCSWG structures and the beam is velocity synchronized to the SIP/TIP, we say that the electron beam is synchronized to three degenerate modes, i.e., we have three-mode synchronization, as was described in [22]. Under the three-mode synchronization regime, the Pierce gain parameter  $C$  will also become larger than that of a conventional SWG TWT due to the enhanced interaction impedance.

## V. CONCLUSION

We have showcased two novel dispersion-engineered three-way SWSs for use in linear electron beam devices: the SLWG and TCSWG geometries. Such geometries are capable of exhibiting SIPs or TIPs in their dispersion relations, and larger

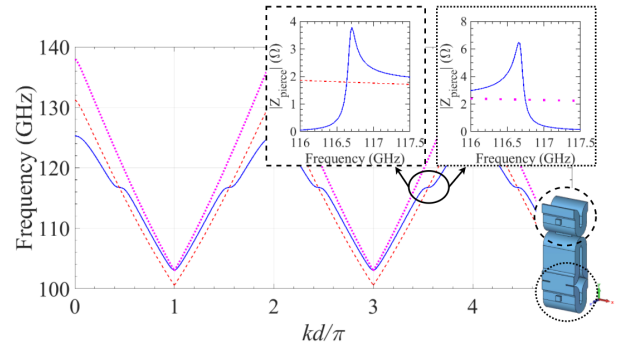


Fig. 7. Pierce (interaction) impedance (solid blue curves) for the top beam tunnel (inset with black dashed border) and bottom beam tunnel (inset with black dotted border) of the TCSWG structure for the eigenmode with a TIP, associated to the circled region in the dispersion diagram showing a nearly-stationary TIP with negative fundamental  $k$  in the  $p = 2$  spatial harmonic (solid blue curve in main figure). The Pierce impedance at the TIP is compared to the Pierce impedance associated with the eigenmodes of the individual serpentine waveguides at the top of the structure (dashed red) and at the bottom of the structure (dotted magenta) when the coupling slots and other waveguide sections are removed. Specifically, the Pierce impedance in both tunnels of the TCSWG structure were calculated over the phase interval  $kd/\pi \in [-0.56, -0.35]$  for the TIP at the appropriate spatial harmonic  $p = 2$ . The dispersion branches of the individual SWG modes associated to the top SWG (dashed red) and bottom SWG (dotted magenta) are also shown in the main figure. The dispersion curves of the main figure were found using the eigenmode solver of CST Studio Suite.

Pierce (interaction) impedance than that of a conventional serpentine waveguide at the frequency corresponding to the inflection point. Using our design methodology, we were able to demonstrate simple conditions which enable one or more SIP/TIP to occur in a three-way waveguide periodic structure once weak periodic coupling is introduced between individual waveguides. We have shown the first known example of a millimeter-wave SWS for linear beam tubes which exhibits stationary or nearly-stationary inflection points in its dispersion relation. A previous example of a waveguide which exhibits an SIP at radio frequencies was demonstrated using microstrip technology in [28], and was the inspiration for this paper.

What is of interest in both of our introduced structures is that the group velocity in the vicinity of the SIP/TIP may be easily controlled by slightly breaking glide-symmetry in our geometries. With weak coupling between waveguides, the dispersion relation of the introduced structures will not be significantly different from the dispersion relations of the individual (uncoupled) waveguides. Due to the “three-mode synchronization” regime, the Pierce impedance, and consequently the Pierce gain parameter, can be drastically enhanced over narrow bandwidths near the SIP/TIP, when compared to a conventional serpentine waveguide commonly used for millimeter-wave TWTs and BWOs. We believe that the introduction of the three-mode synchronization regime in such structures may enable the design of more efficient, compact linear beam tubes, as it was speculated in [22]. There is a lot of room for improvement if one wishes to focus on improving the interaction impedance or bandwidth further using SIPs. However, we believe that the design methodology shown in this paper is still useful for designing realistic millimeter-

TABLE I  
SLWG AND TCSWG DIMENSIONS USED IN FIGURES 4A AND 4B.  
DIMENSIONS ARE IN mm UNLESS SPECIFIED OTHERWISE

	Dimensions used for SWLG	Dimensions used for TCSWG	Notes
$a_t, b_t$	$1.879 - \Delta a/2, a_t/2$	1.726, 0.432	Cross-section dimensions for top waveguide
$a_m, b_m$	$1.879, a_m/6$	1.726, 0.432	Cross-section dimensions for middle waveguide
$a_b, b_b$	$1.879 + \Delta a/2, a_b/2$	1.726, 0.432	Cross-section dimensions for bottom waveguide
$l$	0.940	0.863	Rectangular slot length along x-dimension
$W$	0.100	0.259	Rectangular slot width along z-dimension
$t$	0.100	0.050	Rectangular slot thickness between waveguide bends
$d_t$	0.282	0.259	Width of square beam tunnel
$d$	0.989	1.363	Unit cell pitch
$H_t, H_m, H_b$	$H = 0.784$	$0.472 + \Delta H/2, 1.312, 0.472 - \Delta H/2$	Height of straight sections for top, middle, and bottom SWGs. SLWG only has one $H$ dimension
$u_0/c$	0.200	0.300	Average electron beam velocity normalized to the speed of light

wave SWSs with inflection points in their dispersion relation for use in linear beam tubes. Additionally, we have shown how to obtain TIPs with either backward or forward mode interactions by simply by varying how much glide-symmetry is broken in our structures, potentially enabling the design of either BWOs or TWTs from the same initial geometry. We have also showcased the directional coupler-like properties of both the TCSWG and SLWG structures at frequencies near to the SIP/TIP. This property may be exploited in the design of specialized TWTs or BWOs which can be simultaneously excited from multiple ports or simultaneously drive multiple loads.

#### APPENDIX A DIMENSIONS USED IN FIGURES

For the dispersion of the individual-waveguide ways of the SLWG structure in Fig. 3a (i.e., without coupling), the dimensions are identical to those in Table I with  $\Delta a = 0.1$  mm., with the exception of  $H = 0.843$  mm, which differs from the final  $H$  dimension used for shown in Fig. 4a. Note that, unlike the TCSWG structure, the SLWG structure only has one  $H$  dimension.

For the dispersion of the individual waveguide ways of the TCSWG structure in Fig. 3b, the dimensions are identical to those in Table I with the exception of the normalized beam velocity being  $u_0/c = 0.20$  and the top, middle, and bottom SWG heights being  $H_t = 0.518$  mm,  $H_m = 1.161$  mm, and  $H_b = 0.418$  mm, respectively.

Table I reports the dimensions for Fig. 4a and Fig. 4b as follows. In the inset of Fig. 4a, we have the dimensions used in the SLWG column of Table I, with  $\Delta a = 0.21$  mm for the SIP (black solid lines),  $\Delta a = 0.24$  mm for the alternating-TIP (group velocity alternates in sign at frequencies slightly above or below TIP frequency) (magenta dotted line), and  $\Delta a = 0.18$  mm for the smooth-TIP (group velocity does not change sign at frequencies slightly above or below TIP frequency) (blue dashed line).

In the inset of Fig. 4b, we have the dimensions used in the TCSWG column of Table I, with  $\Delta H = 0.15$  mm for the SIP (black solid line),  $\Delta H = 0.10$  mm for the smooth-TIP (blue dashed line), and  $\Delta H = 0.20$  mm for the alternating-TIP (magenta dotted line).

For the Pierce impedance plot of Fig. 6, we use the dimensions of the SWLG column of Table I, with  $\Delta a = 0.20$  mm, which provides an smooth-TIP that is almost stationary (i.e., it is very close to an SIP). For the Pierce impedance plot of Fig. 7, we use the dimensions of the TCSWG column of Table I, with  $\Delta H = 0.125$  mm, which provides a smooth-TIP that is almost stationary. We simulated the SLWG and TCSWG structures in the eigenmode solver of CST Studio Suite 2019 with a step size of  $0.5^\circ$  in the boundary phase and a tetrahedral mesh setting of 50 cells per max box edge. We found that the peak value of the interaction impedance at an SIP or nearly-stationary TIP for both structures depends greatly on mesh density and step size of boundary phase.

#### APPENDIX B T PARAMETERS

Using frequency-domain simulations, it is possible to rapidly and accurately compute the complex dispersion and approximate finite-length S-parameters of a periodic structure without an eigenmode solver using the frequency-dependent scattering parameters (S parameters) of a single unit cell having separable pairs of ports for each way of the multi-way waveguide structure. The benefit of computing dispersion in this manner is that it is possible to obtain both real and imaginary solutions for the Bloch wavenumber,  $k$ , whereas it is only possible to obtain the real part of the Bloch wavenumber using the eigenmode solver of CST Studio Suite. For lossless and cold structures, the imaginary part of the Bloch wavenumber corresponds to evanescent modes, e.g. below the cutoff frequency of the waveguide or in bandgaps that form where neighboring spatial harmonics meet. It is also notably faster to obtain the unit cell S parameters using the frequency domain solver than it is to directly obtain the modal dispersion from a phase sweep of the periodic boundary in the eigenmode solver. Using this method, it was possible for us to tune the geometry of our structures to obtain beamline synchronism and desired inflection point tilt in a reasonable time frame. The real dispersion obtained by this method was found to be in excellent agreement with CST Studio Suite's eigenmode solutions.

The method we use to obtain the complex dispersion and approximate finite-length S parameters of our periodic structures involves converting between S parameters and scattering

transmission matrices (T parameters) in intermediate steps. T parameters may be directly obtained through algebraic manipulation of each S parameter, as both are defined in terms of the same  $a$ - and  $b$ - waves.

$$\begin{bmatrix} b_1 \\ b_2 \\ b_3 \\ b_4 \\ b_5 \\ b_6 \end{bmatrix} = \mathbf{S} \begin{bmatrix} a_1 \\ a_2 \\ a_3 \\ a_4 \\ a_5 \\ a_6 \end{bmatrix} \iff \begin{bmatrix} b_2 \\ a_2 \\ b_4 \\ a_4 \\ b_6 \\ a_6 \end{bmatrix} = \mathbf{T} \begin{bmatrix} a_1 \\ b_1 \\ a_3 \\ b_3 \\ a_5 \\ b_5 \end{bmatrix} \quad (7)$$

By converting our frequency-dependent S parameters to T parameters at each frequency for the unit cell, it is possible to solve the following Floquet-Bloch eigenvalue problem at each frequency to obtain the complex dispersion diagram for the modes of the periodic structure [42], [70], [71],

$$\mathbf{T}(z + d, z)\Psi(z) = e^{-jkd}\Psi(z),$$

where,  $\Psi$  is the complex state vector for the unit cell composed of  $a$  and  $b$  waves at each port, as shown in Eqn. 7 and Fig. 5a and Fig. 5b, and  $d$  is the unit cell pitch. In other words, the wavenumbers of the fundamental spatial harmonic, may be evaluated directly from the eigenvalues  $\lambda = \exp(-jkd)$  of the T matrix through the relation

$$k = \frac{-\ln(\lambda)}{jd}.$$

The modal dispersion diagrams in Fig. 4a and Fig. 4b (only showing the branches with purely real  $k$ ) are calculated from the eigenvalue problem shown above and are verified using the eigenmode solver of CST Studio Suite. It is also possible to estimate the S parameters of our periodic structure with finite length by cascading T matrices and converting the resultant parameters back into S parameters using the same algebraic manipulation as before [72]. This is how the finite-length S parameters shown in Fig. 5a and Fig. 5b were computed. This method may be readily generalized for  $2N$ -port periodic structures. It is also possible to solve the eigenvalue for spatial harmonics other than the fundamental, as the solutions  $k_n$  are periodic as  $k_n = k + 2\pi n/d$ , with  $n = 0, \pm 1, \pm 2, \dots$

Due to the presence of periodic coupling slots in both of our unit cell designs, our single-cell frequency domain model for our structures must be slightly modified in order to avoid placing ports at coupling slots or in waveguide bends. Our unit cells were modified for the frequency domain solver by horizontally shifting the reference planes of all ports by  $d/4$  along each waveguide path and adding de-embedding to the ports to account for small reflections caused by transitions between straight waveguide sections and waveguide bends and slots, as shown in Fig. 8a and Fig. 8b. This modification does not appear to significantly affect the dispersion relation of the periodic structure under study.

#### ACKNOWLEDGMENTS

This material is based upon work supported by the GAANN Fellowship, by the Air Force Office of Scientific Research under Award FA9550-18-1-0355 and under the MURI Award

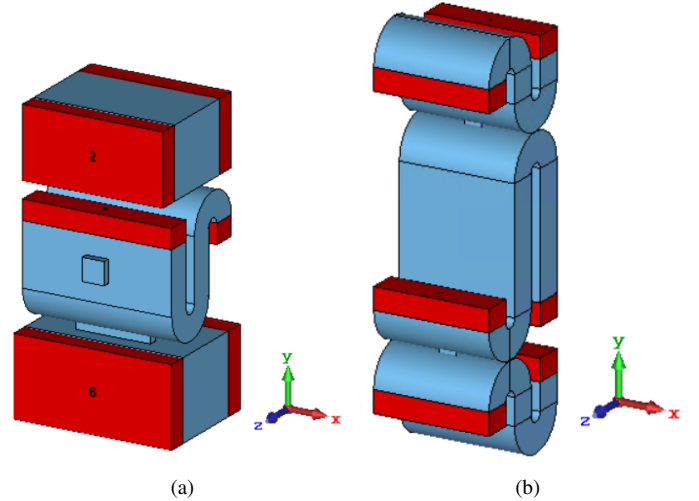


Fig. 8. (a) SLWG and (b) dual-beam TCSWG vacuum unit cells used for calculating the T parameters from the single-cell S parameters. Port reference planes are shifted  $d/4$  along each waveguide path to prevent ports from being placed too close to the coupling slots. Port de-embedding is shown in red. Knowledge of the T matrix allows for fast and accurate calculation of the scattering parameters of multi-way waveguides with several unit cells.

FA9550- 20-1-0409 administered through the University of New Mexico. We thank Dassault Systèmes for providing CST Studio Suite, which has been instrumental in this work. The authors would also like to thank our colleague, Mr. Miguel Saavedra, for his assistance in fixing our interaction impedance calculation.

#### REFERENCES

- [1] J. Pierce, "Waves in electron streams and circuits," *Bell System Technical Journal*, vol. 30, no. 3, pp. 626–651, 1951.
- [2] C. Paoloni, D. Gamzina, R. Letizia, Y. Zheng, and N. C. Luhmann Jr, "Millimeter wave traveling wave tubes for the 21st century," *Journal of Electromagnetic Waves and Applications*, vol. 35, no. 5, pp. 567–603, 2021.
- [3] A. Figotin and I. Vitebskiy, "Electromagnetic unidirectionality in magnetic photonic crystals," *Physical Review B*, vol. 67, no. 16, p. 165210, 2003.
- [4] —, "Gigantic transmission band-edge resonance in periodic stacks of anisotropic layers," *Physical review E*, vol. 72, no. 3, p. 036619, 2005.
- [5] —, "Frozen light in photonic crystals with degenerate band edge," *Physical Review E*, vol. 74, no. 6, p. 066613, 2006.
- [6] —, "Slow-wave resonance in periodic stacks of anisotropic layers," *Physical Review A*, vol. 76, no. 5, p. 053839, 2007.
- [7] —, "Slow light in photonic crystals," *Waves in Random and Complex Media*, vol. 16, no. 3, pp. 293–382, 2006.
- [8] —, "Slow wave phenomena in photonic crystals," *Laser & Photonics Reviews*, vol. 5, no. 2, pp. 201–213, 2011.
- [9] H. Ramezani, S. Kalish, I. Vitebskiy, and T. Kottos, "Unidirectional lasing emerging from frozen light in nonreciprocal cavities," *Physical review letters*, vol. 112, no. 4, p. 043904, 2014.
- [10] M. B. Stephanson, K. Sertel, and J. L. Volakis, "Frozen modes in coupled microstrip lines printed on ferromagnetic substrates," *IEEE microwave and wireless components letters*, vol. 18, no. 5, pp. 305–307, 2008.
- [11] M. A. Othman, F. Yazdi, A. Figotin, and F. Capolino, "Giant gain enhancement in photonic crystals with a degenerate band edge," *Physical Review B*, vol. 93, no. 2, p. 024301, 2016.
- [12] R. Almhadi and K. Sertel, "Frozen-light modes in 3-way coupled silicon ridge waveguides," in *2019 United States National Committee of URSI National Radio Science Meeting (USNC-URSI NRSM)*. IEEE, 2019, pp. 1–2.

- [13] B. Paul, N. K. Nahar, and K. Sertel, "Frozen mode in coupled silicon ridge waveguides for optical true time delay applications," *JOSA B*, vol. 38, no. 5, pp. 1435–1441, 2021.
- [14] G. Mumcu, K. Sertel, and J. L. Volakis, "Lumped circuit models for degenerate band edge and magnetic photonic crystals," *IEEE microwave and wireless components letters*, vol. 20, no. 1, pp. 4–6, 2009.
- [15] M. A. Othman, V. A. Tamma, and F. Capolino, "Theory and new amplification regime in periodic multimodal slow wave structures with degeneracy interacting with an electron beam," *IEEE Transactions on Plasma Science*, vol. 44, no. 4, pp. 594–611, 2016.
- [16] J. R. Burr, N. Gutman, C. M. de Sterke, I. Vitebskiy, and R. M. Reano, "Degenerate band edge resonances in coupled periodic silicon optical waveguides," *Optics express*, vol. 21, no. 7, pp. 8736–8745, 2013.
- [17] M. A. Othman, M. Veysi, A. Figotin, and F. Capolino, "Low starting electron beam current in degenerate band edge oscillators," *IEEE Transactions on Plasma Science*, vol. 44, no. 6, pp. 918–929, 2016.
- [18] M. Y. Nada, M. A. Othman, and F. Capolino, "Theory of coupled resonator optical waveguides exhibiting high-order exceptional points of degeneracy," *Physical Review B*, vol. 96, no. 18, p. 184304, 2017.
- [19] D. Oshmarin, F. Yazdi, M. A. Othman, J. Sloan, M. Radfar, M. M. Green, and F. Capolino, "New oscillator concept based on band edge degeneracy in lumped double-ladder circuits," *IET Circuits, Devices & Systems*, vol. 13, no. 7, pp. 950–957, 2019.
- [20] A. F. Abdelshafy, D. Oshmarin, M. A. Othman, M. M. Green, and F. Capolino, "Distributed degenerate band edge oscillator," *IEEE Transactions on Antennas and Propagation*, vol. 69, no. 3, pp. 1821–1824, 2020.
- [21] A. M. Zuboraj, B. K. Sertel, and C. J. L. Volakis, "Propagation of degenerate band-edge modes using dual nonidentical coupled transmission lines," *Physical Review Applied*, vol. 7, no. 6, p. 064030, 2017.
- [22] F. Yazdi, M. A. Othman, M. Veysi, A. Figotin, and F. Capolino, "A new amplification regime for traveling wave tubes with third-order modal degeneracy," *IEEE Transactions on Plasma Science*, vol. 46, no. 1, pp. 43–56, 2017.
- [23] M. A. Othman, X. Pan, G. Atmatzakis, C. G. Christodoulou, and F. Capolino, "Experimental demonstration of degenerate band edge in metallic periodically loaded circular waveguide," *IEEE Transactions on Microwave Theory and Techniques*, vol. 65, no. 11, pp. 4037–4045, 2017.
- [24] A. Chabanov, "Strongly resonant transmission of electromagnetic radiation in periodic anisotropic layered media," *Physical Review A*, vol. 77, no. 3, p. 033811, 2008.
- [25] T. Mealy and F. Capolino, "General conditions to realize exceptional points of degeneracy in two uniform coupled transmission lines," *IEEE Transactions on Microwave Theory and Techniques*, vol. 68, no. 8, pp. 3342–3354, 2020.
- [26] A. F. Abdelshafy, M. A. Othman, D. Oshmarin, A. T. Almutawa, and F. Capolino, "Exceptional points of degeneracy in periodic coupled waveguides and the interplay of gain and radiation loss: Theoretical and experimental demonstration," *IEEE Transactions on Antennas and Propagation*, vol. 67, no. 11, pp. 6909–6923, 2019.
- [27] D. Oshmarin, A. F. Abdelshafy, A. Nikzamid, M. M. Green, and F. Capolino, "Experimental demonstration of a new oscillator concept based on degenerate band edge in microstrip circuit," *arXiv preprint arXiv:2109.07002*, 2021.
- [28] M. Y. Nada, T. Mealy, and F. Capolino, "Frozen mode in three-way periodic microstrip coupled waveguide," *IEEE Microwave and Wireless Components Letters*, vol. 31, no. 3, pp. 229–232, 2020.
- [29] T. Mealy, A. F. Abdelshafy, and F. Capolino, "High-power backward-wave oscillator using folded waveguide with distributed power extraction operating at an exceptional point," *IEEE Transactions on Electron Devices*, vol. 68, no. 7, pp. 3588–3595, 2021.
- [30] —, "High-power x-band relativistic backward-wave oscillator with exceptional synchronous regime operating at an exceptional point," *Physical Review Applied*, vol. 15, no. 6, p. 064021, 2021.
- [31] —, "Exceptional point of degeneracy in a backward-wave oscillator with distributed power extraction," *Physical Review Applied*, vol. 14, no. 1, p. 014078, 2020.
- [32] A. Figotin and I. Vitebskiy, "Nonreciprocal magnetic photonic crystals," *Physical Review E*, vol. 63, no. 6, p. 066609, 2001.
- [33] A. Figotin and I. Vitebskiy, "Oblique frozen modes in periodic layered media," *Physical Review E*, vol. 68, no. 3, p. 036609, 2003.
- [34] G. Mumcu, K. Sertel, J. L. Volakis, I. Vitebskiy, and A. Figotin, "Rf propagation in finite thickness unidirectional magnetic photonic crystals," *IEEE transactions on antennas and propagation*, vol. 53, no. 12, pp. 4026–4034, 2005.
- [35] M. Sumetsky, "Uniform coil optical resonator and waveguide: transmission spectrum, eigenmodes, and dispersion relation," *Optics Express*, vol. 13, no. 11, pp. 4331–4340, 2005.
- [36] J. Scheuer and M. Sumetsky, "Optical-fiber microcoil waveguides and resonators and their applications for interferometry and sensing," *Laser & Photonics Reviews*, vol. 5, no. 4, pp. 465–478, 2011.
- [37] N. Gutman, C. M. de Sterke, A. A. Sukhorukov, and L. C. Botten, "Slow and frozen light in optical waveguides with multiple gratings: Degenerate band edges and stationary inflection points," *Physical Review A*, vol. 85, no. 3, p. 033804, 2012.
- [38] N. Apaydin, L. Zhang, K. Sertel, and J. L. Volakis, "Experimental validation of frozen modes guided on printed coupled transmission lines," *IEEE transactions on microwave theory and techniques*, vol. 60, no. 6, pp. 1513–1519, 2012.
- [39] H. Li, I. Vitebskiy, and T. Kottos, "Frozen mode regime in finite periodic structures," *Physical Review B*, vol. 96, no. 18, p. 180301, 2017.
- [40] Z. M. Gan, H. Li, and T. Kottos, "Effects of disorder in frozen-mode light," *Optics Letters*, vol. 44, no. 11, pp. 2891–2894, 2019.
- [41] A. Figotin and G. Reyes, "Multi-transmission-line-beam interactive system," *Journal of Mathematical Physics*, vol. 54, no. 11, p. 111901, 2013.
- [42] V. A. Tamma and F. Capolino, "Extension of the pierce model to multiple transmission lines interacting with an electron beam," *IEEE Transactions on Plasma Science*, vol. 42, no. 4, pp. 899–910, 2014.
- [43] D. Hung, I. Rittersdorf, P. Zhang, D. Chernin, Y. Lau, T. Antonsen Jr, J. Luginsland, D. Simon, and R. Gilgenbach, "Absolute instability near the band edge of traveling-wave amplifiers," *Physical review letters*, vol. 115, no. 12, p. 124801, 2015.
- [44] P. Zhang, D. Hung, Y. Y. Lau, D. Chernin, B. Hoff, P. Wong, D. H. Simon, and R. M. Gilgenbach, "Absolute instability near twt band edges," in *2016 IEEE International Vacuum Electronics Conference (IVEC)*. IEEE, 2016, pp. 1–2.
- [45] F. Antoulinakis, P. Wong, A. Jassem, and Y. Lau, "Absolute instability and transient growth near the band edges of a traveling wave tube," *Physics of Plasmas*, vol. 25, no. 7, p. 072102, 2018.
- [46] L. Ang and Y. Lau, "Absolute instability in a traveling wave tube model," *Physics of Plasmas*, vol. 5, no. 12, pp. 4408–4410, 1998.
- [47] M. A. Othman, M. Veysi, A. Figotin, and F. Capolino, "Giant amplification in degenerate band edge slow-wave structures interacting with an electron beam," *Physics of Plasmas*, vol. 23, no. 3, p. 033112, 2016.
- [48] J. W. Gewartowski and H. A. Watson, "Traveling-wave amplifiers," in *Principles of electron tubes: including grid-controlled tubes, microwave tubes, and gas tubes*. Van Nostrand, 1965, ch. 10, p. 357.
- [49] A. K. MM, S. Aditya, and C. Chua, "Interaction impedance for space harmonics of circular helix using simulations," *IEEE Transactions on Electron Devices*, vol. 64, no. 4, pp. 1868–1872, 2017.
- [50] A. Hessel, M. H. Chen, R. C. Li, and A. A. Oliner, "Propagation in periodically loaded waveguides with higher symmetries," *Proceedings of the IEEE*, vol. 61, no. 2, pp. 183–195, 1973.
- [51] M. Bagheriasl, O. Quevedo-Teruel, and G. Valerio, "Bloch analysis of artificial lines and surfaces exhibiting glide symmetry," *IEEE Transactions on Microwave Theory and Techniques*, vol. 67, no. 7, pp. 2618–2628, 2019.
- [52] K. T. Nguyen, A. N. Vlasov, L. Ludeking, C. D. Joye, A. M. Cook, J. P. Calame, J. A. Pasour, D. E. Pershing, E. L. Wright, S. J. Cooke *et al.*, "Design methodology and experimental verification of serpentine/folded-waveguide twts," *IEEE Transactions on Electron Devices*, vol. 61, no. 6, pp. 1679–1686, 2014.
- [53] J. H. Booske, M. C. Converse, C. L. Kory, C. T. Chevalier, D. A. Gallagher, K. E. Kreischer, V. O. Heinen, and S. Bhattacharjee, "Accurate parametric modeling of folded waveguide circuits for millimeter-wave traveling wave tubes," *IEEE Transactions on Electron Devices*, vol. 52, no. 5, pp. 685–694, 2005.
- [54] D. Xu, S. Wang, Z. Wang, W. Shao, T. He, H. Wang, T. Tang, H. Gong, Z. Lu, Z. Duan *et al.*, "Theory and experiment of high-gain modified angular log-periodic folded waveguide slow wave structure," *IEEE Electron Device Letters*, vol. 41, no. 8, pp. 1237–1240, 2020.
- [55] C. Robertson, A. Cross, C. Gilmour, D. Dyson, P. Huggard, F. Cahill, M. Beardsley, R. Dionisio, and K. Ronald, "71-76 ghz folded waveguide twt for satellite communications," in *2019 International Vacuum Electronics Conference (IVEC)*. IEEE, 2019, pp. 1–2.
- [56] E. Backer, W. Ehrfeld, D. Münchmeyer, H. Betz, A. Heuberger, S. Pongratz, W. Glashauser, H. Michel, and R. v. Siemens, "Production of separation-nozzle systems for uranium enrichment by a combination of x-ray lithography and galvanoplastics," *Naturwissenschaften*, vol. 69, no. 11, pp. 520–523, 1982.



- [57] H. Li and J. Feng, "Microfabrication of w band folded waveguide slow wave structure using two-step uv-liga technology," in *2012 IEEE International Vacuum Electronics Conference (IVEC)*. IEEE, 2012, pp. 387–388.
- [58] H. Li, Y. Li, and J. Feng, "Fabrication of 340-ghz folded waveguides using kmpir photoresist," *IEEE electron device letters*, vol. 34, no. 3, pp. 462–464, 2013.
- [59] C. D. Joye, J. P. Calame, M. Garven, and B. Levush, "Uv-liga microfabrication of 220 ghz sheet beam amplifier gratings with su-8 photoresists," *Journal of Micromechanics and Microengineering*, vol. 20, no. 12, p. 125016, 2010.
- [60] S.-T. Han, S.-G. Jeon, Y.-M. Shin, K.-H. Jang, J.-K. So, J.-H. Kim, S.-S. Chang, and G.-S. Park, "Experimental investigations on miniaturized vacuum electron devices," in *IVESC 2004. The 5th International Vacuum Electron Sources Conference Proceedings (IEEE Cat. No. 04EX839)*. IEEE, 2004, pp. 404–405.
- [61] G. Park, Y. Shin, J. So, S. Han, K. Jang, J. Kim, and S. Chang, "Feasibility study of two-step liga-fabricated circuits applicable to millimeter/submillimeter wave sources," in *AIP Conference Proceedings*, vol. 807, no. 1. American Institute of Physics, 2006, pp. 299–308.
- [62] Y.-M. Shin, G.-S. Park, G. P. Scheitrum, and B. Arfin, "Novel coupled-cavity twt structure using two-step liga fabrication," *IEEE transactions on plasma science*, vol. 31, no. 6, pp. 1317–1324, 2003.
- [63] H. Li, J. Cai, Y. Du, X. Li, and J. Feng, "Uv-liga microfabrication for high frequency structures of a y-band twt 2nd harmonic amplifier," in *2015 IEEE International Vacuum Electronics Conference (IVEC)*. IEEE, 2015, pp. 1–2.
- [64] C. D. Joye, J. P. Calame, D. K. Abe, K. T. Nguyen, E. L. Wright, D. E. Pershing, M. Garven, and B. Levush, "3d uv-liga microfabricated circuits for a wideband 50w g-band serpentine waveguide amplifier," in *2011 International Conference on Infrared, Millimeter, and Terahertz Waves*. IEEE, 2011, pp. 1–3.
- [65] A. Gilmour, "Electron motion in static electric fields," in *Principles of traveling wave tubes*. Norwood, MA, USA: Artech House, 1994, ch. 3, p. 20.
- [66] N. J. Fonseca, D. Petrolati, and P. Angeletti, "Design of a waveguide dual-mode three-way power divider for dual-polarization beam forming networks at ka-band," in *2013 IEEE Antennas and Propagation Society International Symposium (APSURSI)*. IEEE, 2013, pp. 1096–1097.
- [67] P. Gardner and B. Ong, "Mode matching design of three-way waveguide power dividers," in *IEE Colloquium on Advances in Passive Microwave Components (Digest No: 1997/154)*. IET, 1997, pp. 5–1.
- [68] G. A. Kumar, B. Biswas, and D. Poddar, "A compact broadband riblet-type three-way power divider in rectangular waveguide," *IEEE Microwave and Wireless Components Letters*, vol. 27, no. 2, pp. 141–143, 2017.
- [69] S. Bhattacharjee, J. H. Booske, C. L. Kory, D. W. Van Der Weide, S. Limbach, S. Gallagher, J. D. Welter, M. R. Lopez, R. M. Gilgenbach, R. L. Ives *et al.*, "Folded waveguide traveling-wave tube sources for terahertz radiation," *IEEE transactions on plasma science*, vol. 32, no. 3, pp. 1002–1014, 2004.
- [70] A. F. Abdelshafy, M. A. Othman, F. Yazdi, M. Veysi, A. Figotin, and F. Capolino, "Electron-beam-driven devices with synchronous multiple degenerate eigenmodes," *IEEE Transactions on Plasma Science*, vol. 46, no. 8, pp. 3126–3138, 2018.
- [71] M. A. Othman and F. Capolino, "Theory of exceptional points of degeneracy in uniform coupled waveguides and balance of gain and loss," *IEEE Transactions on Antennas and Propagation*, vol. 65, no. 10, pp. 5289–5302, 2017.
- [72] W. F. Egan, "Gain," in *Practical RF system design*. John Wiley & Sons, 2004, ch. 2, pp. 7–45.